University of Pennsylvania
ScholarlyCommons

Departmental Papers (ESE) | Department of Electrical & Systems Engineering

1-31-2020

Modulation of Robot Orientation via Leg-Obstacle Contact Positions

Divya Ramesh
University of Pennsylvania

Anmol Kathail
University of Pennsylvania

Daniel E. Koditschek
University of Pennsylvania, kod@seas.upenn.edu

Feifei Qian
University of Pennsylvania

Follow this and additional works at: https://repository.upenn.edu/ese_papers

 Part of the Electrical and Computer Engineering Commons, and the Systems Engineering Commons

Recommended Citation

Divya Ramesh, Anmol Kathail, Daniel E. Koditschek, and Feifei Qian, "Modulation of Robot Orientation via Leg-Obstacle Contact Positions", *IEEE ROBOTICS AND AUTOMATION LETTERS* 5(2), 2054-2061. January 2020. http://dx.doi.org/10.1109/LRA.2020.2970687

Preprint version

This paper is posted at ScholarlyCommons. https://repository.upenn.edu/ese_papers/865
For more information, please contact repository@pobox.upenn.edu.

Modulation of Robot Orientation via Leg-Obstacle Contact Positions

Abstract

We study a quadrupedal robot traversing a structured (i.e., periodically spaced) obstacle field driven by an open-loop quasi-static trotting walk. Despite complex, repeated collisions and slippage between robot legs and obstacles, the robot's horizontal plane body orientation (yaw) trajectory can converge in the absence of any body level feedback to stable steady state patterns. We classify these patterns into a series of "types" ranging from stable locked equilibria, to stable periodic oscillations, to unstable or mixed period oscillations. We observe that the stable equilibria can bifurcate to stable periodic oscillations and then to mixed period oscillations as the obstacle spacing is gradually increased. Using a 3D-reconstruction method, we experimentally characterize the robot leg-obstacle contact configurations at each step to show that the different steady patterns in robot orientation trajectories result from a self-stabilizing periodic pattern of leg-obstacle contact positions. We present a highly-simplified coupled oscillator model that predicts robot orientation pattern as a function of the leg-obstacle contact mechanism. We demonstrate that the model successfully captures the robot steady state for different obstacle spacing and robot initial conditions. We suggest in simulation that using the simplified coupled oscillator model we can create novel control strategies that allow multi-legged robots to exploit obstacle disturbances to negotiate randomly cluttered environments. For more information: Kod*lab (link to kodlab.seas.upenn.edu)

Keywords

Dynamics, Legged Robots, Contact Modeling

Disciplines

Electrical and Computer Engineering | Engineering | Systems Engineering

Comments

Preprint version

This journal article is available at ScholarlyCommons: https://repository.upenn.edu/ese_papers/865

Modulation of Robot Orientation via Leg-Obstacle Contact Positions

Divya Ramesh[1], Anmol Kathail[1], Daniel E. Koditschek[1], and Feifei Qian[1]

***Abstract*—We study a quadrupedal robot traversing a structured (i.e., periodically spaced) obstacle field driven by an open-loop quasi-static trotting walk. Despite complex, repeated collisions and slippage between robot legs and obstacles, the robot's horizontal plane body orientation (yaw) trajectory can converge in the absence of any body level feedback to stable steady state patterns. We classify these patterns into a series of "types" ranging from stable locked equilibria, to stable periodic oscillations, to unstable or mixed period oscillations. We observe that the stable equilibria can bifurcate to stable periodic oscillations and then to mixed period oscillations as the obstacle spacing is gradually increased. Using a 3D-reconstruction method, we experimentally characterize the robot leg-obstacle contact configurations at each step to show that the different steady patterns in robot orientation trajectories result from a self-stabilizing periodic pattern of leg-obstacle contact positions. We present a highly-simplified coupled oscillator model that predicts robot orientation pattern as a function of the leg-obstacle contact mechanism. We demonstrate that the model successfully captures the robot steady state for different obstacle spacing and robot initial conditions. We suggest in simulation that using the simplified coupled oscillator model we can create novel control strategies that allow multi-legged robots to exploit obstacle disturbances to negotiate randomly cluttered environments.**

***Index Terms*—Dynamics, Legged Robots, Contact Modeling**

I. INTRODUCTION

ANIMALS often use limb and body contact to negotiate complex, cluttered environments. Snakes can use their body segments to push against grass stems to change their direction of movement [1], [2]. Cockroaches have been found to use different pitch and roll body angles to traverse dense, tall grass-like barriers of varying stiffness [3], [4]. Human beings also instinctively coordinate their limbs to take advantage of obstacle collisions in locomotion tasks such as parkour.

In contrast, robots typically avoid most collisions and contacts with their physical environments and treat large disturbances as "obstacles" because our limited understanding of contact reaction forces precludes their effective use. Without a better understanding of the dynamics of repeated locomotor-obstacle interactions [3], [5], [6] methods and strategies developed for flat, smooth ground are often not directly applicable. Recent robophysics studies demonstrate the great potential of obtaining such understanding from systematic experiments in simplified settings [7], [8], [9], [10], [11], [12], [5], [13]. While the vast parameter space presented by any natural environment presents daunting challenges to analysis, this paper seeks to build on recent progress in extracting a highly abstracted but physically revealing model of periodic legged gaits interacting with periodically structured obstacle fields [13]. Our central goal in this paper is to refine this model to explain a broader set of interaction patterns while maintaining a sufficiently abstract representation to permit control strategies that might use them systematically for navigation. Specifically, we study a quadrupedal robot engaging a periodically spaced field of half-cylindrical obstacles using a low-frequency trotting walk in a manner laid out as follows. Sec. II describes the experiment setup and data processing algorithms. In Sec. III, we first report on the appearance and disappearance of "types" of stable steady state patterns of the robot's yaw trajectory that emerge as the obstacle spacing is gradually increased. We then show how to refine the original model [13] to successfully predict this observed series of pattern bifurcations. We end that section by presenting a speculative use of this model for an active gait controller whose simulation suggests that it might allow a robot to exploit obstacle disturbances to effectively navigate in a randomly-structured obstacle-filled environment. Sec. IV briefly reviews the contributions and offers a brief sketch of future work.

Manuscript received: September, 10, 2019; Revised December, 14, 2019; Accepted January, 11, 2020.

This paper was recommended for publication by Editor Dezhen Song upon evaluation of the Associate Editor and Reviewers' comments.

*This research was supported by the National Science Foundation (NSF) under INSPIRE award, CISE NRI 1514882 and NRI INT award 1734355.

[1]All Authors are with Electrical and Systems Engineering, University of Pennsylvania, Philadelphia, PA 19104, USA fqian@seas.upenn.edu

Digital Object Identifier (DOI): see top of this page.

II. EXPERIMENTAL MATERIALS AND METHODS

To simplify the complexity of the natural cluttered environment, and to begin extracting key mechanisms of robot locomotion dynamics under modulation of a contact-rich environment, in this study we perform systematic experiments to investigate the steady-state dynamics of robot-obstacle interactions in a periodically-structured environment. In this section, we introduce the experimental setup (Sec. II-A) and data analysis protocols (Sec. II-B) that allow us to reveal fundamental interaction principles and develop phenomenological abstract reduced-order models (Sec. III-B) of the coupled dynamics. We later demonstrate that these highly abstracted insights, although developed from simplified and structured settings, can lead to innovative control strategies applicable in randomly-structured environments (Sec. III-D).

A. Experiment Setup

1) Robot: A hexapedal robot, HQRHex (Fig. 1C), was used to perform all experiments in this paper. HQRHex[1]is a smaller version (0.48 m in length and 0.29 m in width) of

the C-legged RHex class robots [14]. Each leg is attached to a gearless direct-drive motor [15] (Tiger Motor U8) which provides a fast and accurate torque estimation during the robot's interaction with the obstacles. The leg motors are controlled by a customized micro-controller (Ghost Robotics MBLC v0.5.2). The robot is powered using a 6400 mAh 4-cell LiPo battery (16.8 V when fully charged).

For this study, the robot was programmed to function as a quadruped (the two middle legs held up in the air and not engaged in locomotion) during obstacle field traversing. A common quadrupedal gait, trotting (one pair of the diagonal legs move together and alternate with the other pair of diagonal legs (Fig. 1D)), was implemented on the robot as it interacts with the obstacle field, with a stride frequency of 0.27 Hz.

2) Environment: An array of 15 evenly-spaced half-cylinders (Fig. 1A, B) were used as a simplified form of obstacle-filled environment for our experiments. This structured environment allows for systematic control and variation of environment parameters and facilitated the emergence of passive (i.e., without any body-level feedback control) robot orientation steady states under repeated obstacle disturbances. The obstacle diameter is $D = 0.11$ m, comparable to the robot leg size. The obstacle spacing was systematically varied between 2.5 inches and 6.5 inches with 1-inch intervals (corresponding to five different obstacle spacings of 0.06 m, 0.09m, 0.11m, 0.14m, and 0.17m).

3) Data collection: For each of the five obstacle spacings, 24 trials were performed with systematically-varied robot initial conditions. The initial orientation of the robot, θ_i, was varied from 0 degrees to 70 degrees. The fore-aft direction initial position of the robot, I, was varied from $I = 0.5$ m to $I = 0.9$ m. This fore-aft position of the robot was defined as the distance between the robot's right front leg and the near edge of the first obstacle. Due to the symmetry in the environment along the lateral direction, we only investigate and discuss $\theta_i > 0$ region and assume symmetry for the $\theta_i < 0$ region.

Two types of measurements, Motion Capture (MoCap) tracking and microcontroller logging, were collected and synchronized for each trial. The motor angular positions and torques were logged with the robot's microcontroller (Ghost Robotics MBLC v0.5.2), whereas robot Center of Mass (CoM) 6 degree-of-freedom (DoF) positions (Fig. 1B) were tracked by the MoCap system (Vicon).

B. Data Analysis

1) Orientation state characterization: The steady yaw angle of the robot, θ_f, is used to characterize different steady-state behaviors into "types" which will be further discussed in Sec. III. This angle is calculated by averaging the yaw angle of the robot during the stabilized region of the robot-obstacle interaction from the experimental data. The stabilized region is selected as the last 1m of the robot trajectory in the obstacle field, before either of the front leg exits the boundary. The statistics reported in Sec. III-A and Table I represents the mean $\pm$ standard deviation of θ_f computed from all trials for the corresponding type of steady state within each obstacle spacing.

[1]The robot was used as a simplified model system in this study to allow systematic parameter variation and to facilitate the understanding the complex coupled dynamics of robot-obstacle interactions. We expect that the coupled oscillator model (Sec. III-B) and the "obstacle-aided navigation" concept (Sec. III-D) developed using this model system can later be applied to more general multi-legged platforms with different designs.

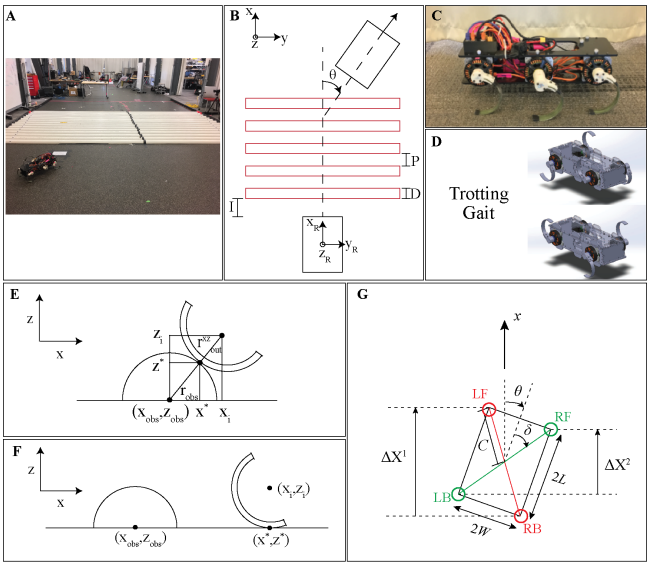

Figure 1. Experiment setup and contact position detection method to investigate the dynamics of a legged robot interacting with a regular obstacle field. (A) Experiment setup of the obstacle field. (B) The obstacle field consists of half-circular pipes of diameter D, regularly spaced with distance P. For each trial the robot begins from systematically varied initial orientation (yaw) angles θ_i and fore-aft distances I. (C) HQRHex is a small RHex [14] class robot with the middle legs held in air during all trials so that it functions as a quadruped. (D) The robot uses a feed-forward trotting gait (one pair of the diagonal legs move together and alternate with the other pair of diagonal legs) to traverse the obstacle field. The periodic gait couples with the periodically-structured environment and allows the emergence of passive steady state dynamics. (E) Point of Contact on the obstacle. (F) Point of contact on the flat ground. (G) Coupled oscillator model (Sec. III-B) diagram.

2) Contact Position Analysis: To understand the emergence of different steady states during periodic robot-obstacle interactions, the initial contact positions of each leg with the obstacle was computed as the robot trotted over the obstacle field. In this subsection, we briefly overview the method used to extract these contact positions from the experiment data.

a) 3-D Reconstruction: A 3-D reconstruction of the experiment was used for the identification of contact position patterns to study the robot-obstacle interaction. The robot body and obstacles were reconstructed using the MoCap-tracked CoM positions. At every time step, the robot was transformed to its pose in the world frame using transformation matrices calculated from the MoCap tracking data. The legs were then reconstructed relative to the body based on the actual motor angular position, β_{mot}.

b) Estimation of contact point on the leg: Once the robot legs and obstacles were reconstructed, the obstacle in contact with each leg was identified by the following criterion:

$$k_c = \arg\min_k |x_{obs}(k) - x_i| \tag{1}$$

here $k \in [1, 15]$ denotes obstacle index, k_c denotes the obstacle in contact, x_i is the fore-aft position of leg i. The algorithm then automatically identifies all leg-obstacle contact events by finding peaks in the motor torque, τ_{mot}. For each contact event, we calculate the euclidean distance, d, between leg i and obstacle k_c:

$$d = \sqrt{(x_i - x_{obs})^2 + (z_i - z_{obs})^2} \tag{2}$$

where x_i, z_i are the fore-aft and vertical positions of the leg center, x_{obs} and z_{obs} are the fore-aft and vertical positions of obstacle k_c.

We define the contacting threshold, d_c, to be the sum of the radius of the obstacle, r_{obs}, and the outer radius of the leg i projected onto the X-Z plane, r^{xz}_{out}:

$$d_c = (r_{obs} + r^{xz}_{out}) \tag{3}$$

If $d <= {d_c}^2$, we classify leg i to be in contact with obstacle k_c (Fig. 1E), and calculate the contact position on the obstacle using the triangle proportionality theorem:

$$x^* = \frac{r_{obs}x_i + r^{xz}_{out}x_{obs}}{r_{obs} + r^{xz}_{out}},\ z^* = \frac{r_{obs}z_i + r^{xz}_{out}z_{obs}}{r_{obs} + r^{xz}_{out}} \tag{4}$$

$$y^* = y_i \tag{5}$$

If $d > d_c$, we classify leg i to be in contact with the flat ground (Fig. 1F), and the contact position is given by

$$x^* = x_i,\ y^* = y_i,\ z^* = z_{obs} \tag{6}$$

III. RESULTS AND DISCUSSION

Using the experiment setup and data analysis methods discussed in Sec. II, we investigate how the coupled dynamics between robot and obstacles is modulated by leg-obstacle contact position patterns, and how such modulation principle could be used to allow obstacle-aided locomotion and navigation.

The dynamics of locomotion by a multi-legged robot undergoing repeated perturbations from obstacle interactions is nontrivial. At any step, small changes in leg-obstacle contact positions could result in variation in robot orientation, which can lead to substantial changes in the contact position at the next step, causing the robot to switch to a completely different trajectory [6].

Despite such complexity, we noticed from our experiments that periodic robot gaits seem to couple with periodically structured environments and produce stable, periodic dynamics. The emergence of such periodic behaviors allows us to closely observe how the dynamics of robot orientation are governed by repeated leg-obstacle interactions, lending increasing insight into the consequences of their interaction for overall body motion.

In Sec. III-A we present the different steady-state behaviors observed from experiments, and the passage from one to another as obstacle spacing is gradually increased. These observations suggest a very simple model incorporating our hypothesized stability mechanism as discussed in Sec. III-B. We compare the predictions of this model against the measured experimental data in Sec. III-C, and offer speculative remarks of the prospects for using this model for planning active control policies for randomized obstacle fields in Sec. III-D.

A. Stability of the types of orientation steady states

Fig. 2 shows the horizontal-plane trajectories of the robot CoM traversing through obstacle fields with different spacings. We noticed that the robot's orientation exhibited several distinct types of steady-state dynamics, including both consistent orientation as if in equilibrium and periodic oscillation.

The trajectories of the robot converge from different initial orientation angles to these steady-state behaviors in a manner characteristic of the classical dynamical systems notion of an attractive basin. The trajectories with similar orientation angles and same qualitative leg-obstacle contact patterns during the stabilized region were classified into the same steady state type group. This qualitative classification yields five different types of steady states with each having a distinct stabilizing mechanism. The type labels associated with the groupings of curves in Fig. 2 are interpreted in Table I in terms of the roughly constant (**Type I, III, V**) or roughly periodic oscillations (**Type II, IV**) of steady state yaw.

Fig. 3 shows the fixed points (markers) for the five different types of steady states, with the the basin of attractions (colored regions) – in reminiscent of a bifurcation diagram – that converges to these states. As the obstacle spacing is increased, the stability and the size of basin of attraction for each steady state type varies.

At spacing P = 0.06 m, **Type I** (equilibrium steady state at $|\theta_f| = 5.6^\circ \pm 0.8^\circ$), **Type III***[4] (the oscillatory steady-state at $|\theta_f| = 37.7^\circ \pm 4.3^\circ$) and **Type V**[5](the equilibrium steady-state at $|\theta_f| = 94.0^\circ \pm 0.7^\circ$) was observed (Fig. 2A, Fig. 3). We noticed that in some of the trajectories, the robot would temporarily move along $\approx 30^\circ$ but would eventually converge to $\approx 0^\circ$ due to the intrinsic experimental noise indicating that **Type I** steady state is more stable than **Type III*** at this spacing.

As spacing increased from P = 0.06 m to P = 0.09 m, **Type I** equilibrium bifurcated into **Type II** ($|\theta_f| = 7.5^\circ \pm 1.5^\circ$) periodic oscillatory state, while **Type III** ($|\theta_f| = 34.7^\circ \pm 0.4^\circ$) and **Type V** ($|\theta_f| = 94.7^\circ \pm 0^\circ$) persist (Fig. 2B, Fig. 3). **Type III** steady state became more stable at this spacing than at $P = 0.06$ m.

[2] $d < d_c$ occurs when the concave side of the half-circular leg is "hugging" the convex obstacle

[3] Intrinsic experiment noise can cause some less stable types (e.g., Type III* in Fig. 2A) to switch to more stable types (e.g., Type I). Type labels in Fig. 2 aims at providing rough visual correspondence and do not intend to capture such exceptions.

[4] We use the symbol $\star$ to denote less stable states, or possible non-periodic oscillations. Experimental confirmation was difficult since small amounts of noise could easily interfere with the (theoretically) periodic pattern of dynamics (like the case with **Type II***), or shift it to the attraction basin of other equilibrium states (like the case with **Type III*** here). A complete understanding of simpler steady states with a more delicate experiment setup is needed to make further study of these more complex dynamics.

[5] The 90° equilibrium state is a trivial case that was already observed and discussed in [13]. In this steady state all robot legs stepped on the flat ground between the obstacles while the robot walked sideways. Since the mechanism is trivial we will not analyze it further here and only include the observation for completeness.

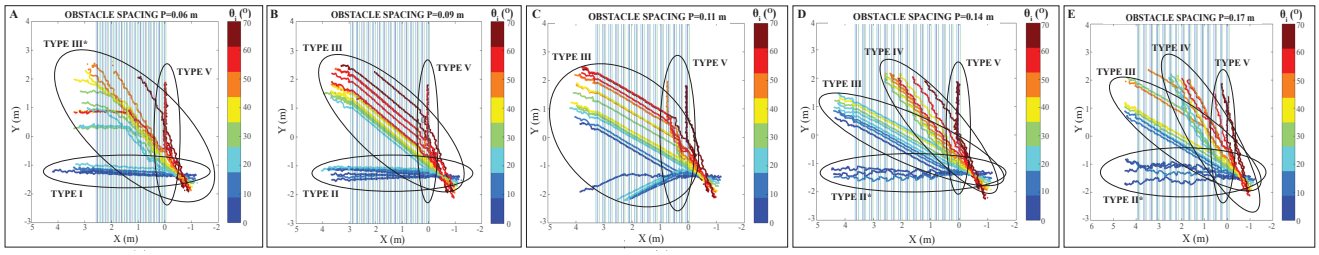

Figure 2. Trajectories of the robot's center of mass on the XY plane at different obstacle spacings P with systematically varied initial orientation angles θ_i. Type labels in the figures loosely[3] correspond to different steady state behaviors as summarized in Table I. (A) P = 0.06 m; (B) P = 0.09 m; (C) P = 0.11 m; (D) P = 0.14 m; and (E) P = 0.17 m. Color indicates initial orientation angles θ_i.

Table I
TYPES OF STEADY STATES.

Type (Fig. 2)	**Steady State Pattern (Stability)**	**Obstacle Spacing (m)**	**Mechanism** (Fig.4(iv), Eqn. 12, 14)		**Steady Yaw** $\lvert\theta_f\rvert$ (°)
			Step 1	**Step 2**	
I	Equilibrium	0.06	RF and LB slip forward, no turning	LF and RB slip forward, no turning	5.6 ± 0.8
II / II*	Periodic Oscillations (stable)	0.09	Only RF slips forward, CCW turning	Only LF slips forward, CW turning	7.5 ± 1.5
	Oscillations (less stable)	0.14			6.6 ± 1.0
	Oscillations (less stable)	0.17			6.4 ± 4.2
III / III*	Oscillations (less stable)	0.06	Both step on ground, no turning	Both step on ground, no turning	37.7 ± 4.3
	Equilibrium (stable)	0.09			34.7 ± 0.4
	Equilibrium (stable)	0.11			30.9 ± 0.2
	Equilibrium (stable)	0.14			31.8 ± 0.1
	Equilibrium (stable)	0.17			30.4 ± 0.9
IV	Periodic Oscillations (stable)	0.14	Only RF slips forward, CCW turning	Only RB slips forward, CW turning	63.9 ± 3.2
	Periodic Oscillations (stable)	0.17			63.1 ± 3.0
V	Equilibrium (stable)	0.06	Both step on ground, no turning	Both step on ground, no turning	94.0 ± 0.7
	Equilibrium (stable)	0.09			94.7 ± 0.0
	Equilibrium (stable)	0.11			93.7 ± 1.8
	Equilibrium (stable)	0.14			96.2 ± 1.3
	Equilibrium (stable)	0.17			85.2 ± 6.8

Types of **Steady State Patterns** of yaw trajectories associated with the groupings of COM trajectories labeled in Fig. 2. Asterisks denote type variants exhibiting qualitatively less stability. CCW refers to counter-clock wise. CW refers to clock wise. Hypothesized stability **Mechanism** for each type is detailed in Fig. 4(iv). **Steady Yaw**, θ_f, is roughly constant for equilibrium patterns (filled circles of Fig. 3) and roughly the mean yaw for periodic patterns (open circles of Fig. 3).

As spacing kept increasing from P = 0.09 m to P = 0.11 m, **Type II** was no longer observed in experiments (Fig. 2C, Fig. 3). **Type III** ($|\theta_f| = 30.9° \pm 0.2°$) appeared to be the most stable equilibrium at this spacing, with the largest basin of attraction (from approximately 0° to 60°). **Type V** equilibrium ($|\theta_f| = 93.7° \pm 1.8°$) persists at this spacing.

At even larger spacing (P = 0.14 m and P = 0.17 m, Fig. 2D and E, Fig. 3), **Type II*** ($|\theta_f| = 6.6° \pm 1.0°$ for P = 0.14 m and $|\theta_f| = 6.4° \pm 4.2°$ for P = 0.17 m) became less stable, **Type III** equilibrium ($|\theta_f| = 31.8° \pm 0.1°$ for P = 0.14 m and $|\theta_f| = 30.4° \pm 0.9°$ for P = 0.17 m) persists with a reduced size of basin, and a new steady state, **Type IV** (periodic oscillation around $|\theta_f| = 63.9° \pm 3.2°$ for P = 0.14 m and $|\theta_f| = 63.1° \pm 3.0°$ for P = 0.17 m), emerged. **Type V** ($|\theta_f| = 96.2° \pm 1.3°$ for P = 0.14 m and $|\theta_f| = 85.2° \pm 6.8°$ for P = 0.17 m) persists.

B. Contact position hypothesis and coupled oscillator model

We noticed from experiments that after the robot's orientation stabilized, the alternating pairs of legs also began to repeat a pattern of obstacle contact positions. We hypothesize that the periodic change in the robot orientation during steady states was primarily a result of the synchronization of the contact positions between the two alternating leg pairs.

Based on these experimental results, we now introduce a highly abstracted phenomenological "coupled oscillator model" to initiate formal reasoning about the empirically observed emergence of the various types of steady state behavior documented above. As with the original RHex robot [14], HQRHex robot's gait is generated by a single, centralized, feed-forward "clock", split out into an in-phase and anti-phase reference to drive the virtual biped realized by the robot's alternating diagonally paired hips [16]. Thus the key theoretical question to address concerns the manner in which steady state body yaw emerges from the dynamical coupling between that internal oscillator and the external oscillatory forces arising from leg contact with the spatially periodic ground [17].

We develop a half-stride return map [18] to facilitate in a manner analogous to [19] analysis of the symmetry enforced

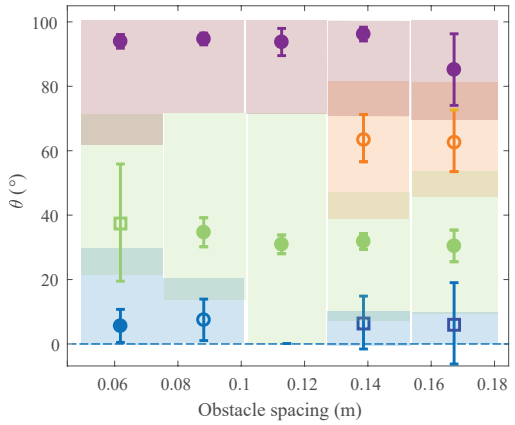

Figure 3. Fixed point and basin of attraction for the five types of robot orientation steady states observed at different obstacle spacing from experiment measurements. Markers indicate fixed points of the orientation steady states. Error bars indicate the range of orientations during oscillations around the fixed points after reaching a steady state. Shaded boxes demarcate approximate basin of attraction (i.e. interval of initial angles, θ_i that converge) around the fixed point of the corresponding color. The shape of markers indicates our classification of steady state dynamics listed in Table I: solid circles indicate equilibrium; open circles indicate stable, periodic oscillations; open squares indicate less stable oscillations.

or broken by the ground geometry across a full stride. We find it convenient to work directly in body yaw coordinates, whereby the pair[6] (θ_k^1, θ_k^2) denotes the robot body's yaw angle (in the inertial world frame) sampled in stride k at the two successive half stride events of interest: initial ground contact by the synchronized leg pair O_1 = {LF, RB} (red, Fig. 1G); and then by O_2 = {RF, LB} (green, Fig. 1G). At each such half stride event, the yaw angle is rigidly related to the difference in fore-aft distance between the contact positions on the obstacle of the corresponding diagonal leg pair:

$$\begin{aligned} \triangle X^1 &= X_{LF} - X_{RB} \\ \triangle X^2 &= X_{RF} - X_{LB}. \end{aligned} \tag{7}$$

In contrast, the phase of ground contact, $\bar{X}_i := X_i \mod P + D$ [13], is advanced at each half-stride by the projected fore-aft step length $S_0' = S_0 cos\theta$ (where S_0 is the constant step length in the robot frame),

$$\begin{aligned} \bar{X}_{k+1}^1 &= (X_{k,i}^2 + S_0 \cos\theta_k^2) \mod P + D \\ \bar{X}_{k+1}^2 &= (X_{k+1,i}^1 + S_0 \cos\theta_{k+1}^1) \mod P + D. \end{aligned} \tag{8}$$

Finally, the resulting yawing torque, representing the crucial coupling between the phase of the periodic ground geometry encountered by the legs with the phase of the trotting cycle when so encountered, arises from the difference in the slipping distances between the two legs. Observing that the slipping distance, $S_i, \quad i \in \{LF, RF, LB, RB\}$, can be represented as a function of the phase of contact [13], we have [7]

$$\begin{aligned} \triangle S_k^1 &= S_{LF}(\bar{X}_{LF}) - S_{RB}(\bar{X}_{RB}) \\ \triangle S_k^2 &= S_{RF}(\bar{X}_{RF}) - S_{LB}(\bar{X}_{LB}). \end{aligned} \tag{9}$$

Computing the differences (7) associated with (8), adding in the slip-induce coupling forces (9), now yields our discrete dynamical system that we write in yaw angle coordinates as

$$\begin{aligned} \theta_{k+1}^1 &= \pm^8 \cos^{-1}[\cos(\theta_k^2 + \delta) + \frac{2W}{C}\sin(\theta_k^2) - \frac{1}{2C} \triangle S_k^2] + \delta \\ \theta_{k+1}^2 &= \pm \cos^{-1}[\cos(\theta_{k+1}^1 - \delta) - \frac{2W}{C}\sin(\theta_{k+1}^1) \\ &\quad + \frac{1}{2C} \triangle S_{k+1}^1] - \delta. \end{aligned} \tag{10}$$

Here L and W are the robot half body length and half body width, $C = \sqrt{L^2 + W^2}$ is the robot's half diagonal length, and $\delta = tan^{-1}(W/L)$ is the aspect ratio angle (Fig. 1G).

C. Comparison of synchronization patterns between experiment and model

We now use the model (10) to exhibit sufficient conditions for a fixed point (i.e. where both half strides repeat the same yaw angle) and a period-two orbit (i.e. where the yaw angle oscillates between the two half strides). We observe in Fig. 4(ii), (iii) that these steady state conditions closely predict the empirical observations. Work in progress will explore conditions for still higher period orbits and develop stability conditions to predict their emergence.

1) Synchronization Mechanism of Equilibrium Types: We define the orientation equilibrium to be:

$$\begin{aligned} \theta_{k+1}^1 &= \theta_k^2 \\ \theta_{k+1}^2 &= \theta_{k+1}^1. \end{aligned} \tag{11}$$

From the model we can derive that one sufficient condition to achieve equilibrium would be:

$$\begin{aligned} \triangle S_k^2 &= 0 \\ \triangle S_{k+1}^1 &= 0. \end{aligned} \tag{12}$$

Fig. 4A shows that as the model predicts, during the steady region of **Type I** equilibrium state (black box in Fig. 4A-(ii),(iii)) both synchronized leg pairs ([RF, LB] and [LF, RB]) contacted between the top and far edge of the obstacle (Fig. 4A-(ii),(iii),(iv)) and slips forward the same amount (Eqn. 12), allowing the robot to maintain a constant orientation at 0° (Eqn. 11, Fig. 4A-(i)) despite the repeated obstacle disturbances. This is consistent with previous observations from [13].

Similar to **Type I**, in **Type III** equilibrium, during the steady region (black box in Fig. 4C-(ii),(iii)), both synchronized leg pairs ([RF, LB], [LF, RB]) steps either on the flat

[6]Here and throughout the sequel, we use the subscript, k, to denote the stride number, whereas superscripts denote the 1^{st} and 2^{nd} half-stride events, respectively.

[7]excluding the special condition of $\triangle Y^1 = Y_{LF} - Y_{RB} = 0$ and $\triangle Y^2 = Y_{RF} - Y_{LB} = 0$, in which case we have $\triangle S_k^1 = 0$ and $\triangle S_k^2 = 0$, respectively.

[8]the model selects one of the solution based on the value of $\triangle S$ and the pre-slip robot orientation.

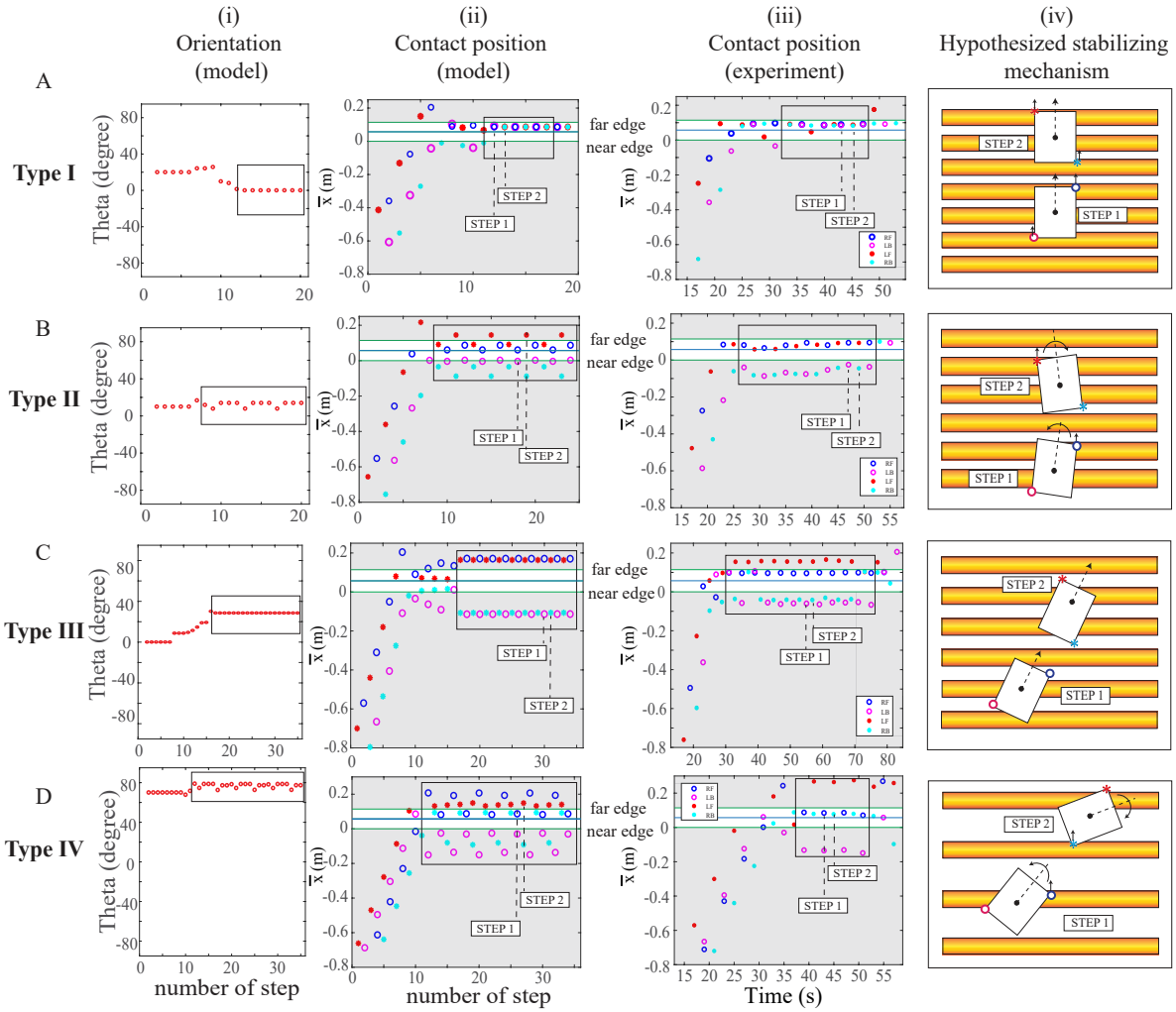

Figure 4. Comparison of leg-obstacle contact point pattern from model and experiment for different types of steady states. (A) Contact point pattern for **Type I** steady states at obstacle spacing of 0.06 m. (i) Model-predicted robot orientation. (ii) Model-predicted contact point pattern. (iii) Experimentally characterized contact position pattern. In both (ii) and (iii), $\bar{x}$ denotes the normalized fore-aft position relative to the near edge of the contacting obstacle. The green boundary of the white space represent the near edge ($\bar{x} = 0$) and far edge ($\bar{x} = D$) of the obstacle. The blue centerline of the white space represent the top of the obstacle where the direction of leg slippage switches[6], [13]. The markers indicate the normalized initial leg contact position on the obstacle: blue circle indicates the normalized initial obstacle-contact position of the RF leg; red star indicates the normalized initial obstacle-contact position of the LF leg; Magenta circle indicates the normalized initial obstacle-contact position of the LB leg; cyan star indicates normalized initial obstacle-contact position of the RB leg. Gray shaded region in (ii) and (iii) indicate flat ground where obstacle disturbance and leg slippage is zero. (iv) Illustrative diagram of stabilizing mechanism. Black boxes in (i)-(iii) indicate stabilized region of steady state. Orange region in (iv) represent obstacles. (B) Contact point pattern for **Type II** steady states at obstacle spacing of 0.09 m. (C) Contact point pattern for **Type III** steady states at obstacle spacing of 0.11 m. (D) Contact point pattern for **Type IV** steady states at obstacle spacing of 0.17m. In (B)-(D), content of sub-figures, notations, and marker representations are the same as (A).

ground between the obstacles, or at the edge of the obstacles (Fig. 4C-(ii),(iii)). In either case, the difference in slippage within the synchronized leg pair is approximately zero (Eqn. 12), allowing the robot to maintain a constant orientation at approximatley $\pm 30^\circ$ (Eqn. 11, Fig. 4C-(i)). This stable orientation depends sensitively on obstacle spacing, and can be analytically calculated using the ODF framework presented in [13].

2) Synchronization Mechanism of Period-2 Oscillations Types: We define the discrete, period-2 oscillation of orientation as:

$$\begin{aligned} \theta^1_{k+1} &= \theta^1_k \\ \theta^2_{k+1} &= \theta^2_k. \end{aligned} \tag{13}$$

One sufficient condition for this type of steady state would be:

$$\begin{aligned} \triangle S^1_{k+1} - \triangle S^2_k &= 4W(\sin\theta^1_{k+1} - \sin\theta^2_k) \\ \triangle S^2_{k+1} - \triangle S^1_{k+1} &= 4W(\sin\theta^2_{k+1} - \sin\theta^1_{k+1}) \end{aligned} \tag{14}$$

In the periodic oscillatory steady state **Type II** (Fig. 4B), during the first half of the stride (labeled "STEP 1" in Fig. 4 (ii)-(iv)), leg pair [RF, LB] (O_1) is in stance. Leg RF (blue circle in Fig. 4B-(ii),(iii)) contacts the obstacle between the top and far edge and slips forward, whereas LB (magenta circle in Fig. 4B-(ii),(iii)) steps on flat ground and no slip occurs. The resulting total disturbance causes the robot to turn counterclockwise (Fig. 4B-(iv) step one). Similarly, during the second half of the stride (labeled "STEP 2" in Fig. 4 (ii)-(iv)), leg pair [LF, RB] (O_2) is in stance. Leg LF (red

star in Fig. 4B-(ii),(iii)) contacts the obstacle between the top and far edge and slips forward, whereas RB (cyan star in Fig. 4B-(ii),(iii)) steps on flat ground and no slip occurs. The resulting total disturbance causes the robot to turn clockwise (Fig. 4B-(iv) step two). The repetition of this contact position pattern resulted in the observed periodic oscillation of the robot orientation (Eqn. 13, Fig. 4B-(i)).

Similar to **Type II**, the oscillation of robot orientation observed in **Type IV** was a result of the two oscillators, O_1 and O_2, generating a turning moment in same magnitude but opposite directions (Eqn. 14, Fig. 4D-(iv)). The periodic repetition of this movement caused the observed oscillation in robot orientation angle (Eqn. 13, Fig. 4D-(i)).

We note that the highly-abstracted model aims to capture and understand the dominant coupling dynamics between robot and obstacles, and therefore does not take into account many details such as leg compliance, and periodic movement of leg relative to the hip. These simplifications lead to some discrepancies between model prediction and experiment observations. For example, we notice that the amount of orientation oscillation appears to be smaller in experiment (1.5°) as compared to predicted in model (3.5°). In addition, orientation and contact phase in experiments exhibit period-two oscillation rather than period-four in simulation. This is likely due to the model's assumption that the legs are completely rigid, but the c-shaped legs used in experiments can compress and "damp out" some of the obstacle disturbances. Future work shall explore the sensitivity of different steady states to noises.

D. Broader applicability: Gait sequence planning in a random obstacle field

The model provides a simple yet effective representation that allows reasoning about how multi-legged robots could produce different dynamics within the same environment by controlling the pattern of leg-obstacle interactions. In this section we demonstrate in simulation that without active steering, a quadrupedal robot could adjust its gait sequence to produce different obstacle-aided navigation patterns from a random obstacle field. The idea is that a robot would reactively select legs to engage obstacles in a manner such that the total obstacle disturbance is in favor of the robot's locomotion goal. At each step, the model evaluates the potential slippage that a leg could produce if the leg was chosen to engage with the available obstacle at its position. Based on this evaluation the model selects the set of legs that could produce the most progress towards the desired locomotion goal. Here we demonstrate four different navigation patterns: counter-clockwise turning (Fig. 5A), clockwise turning (Fig. 5B), moving straight (Fig. 5C), and zig-zag (Fig. 5D).

Taking the counter-clockwise turning as an example, at each step the model selects the leg from the right side with a maximal forward-slipping disturbance during the obstacle interaction and selects the leg from the left side with maximal backward-slipping disturbance. The selected legs would then get activated to engage with the obstacle, producing a counter-clockwise turning moment, while the other legs stay in the aerial pose. The model predicts the robot orientation after the leg slippage, moves the robot one step length forward along the new orientation and repeats to evaluate potential slippage for all legs and choose the activated leg group for the next step. For the clockwise turning behavior, the process is similar, except that the model selects the leg with maximal backward slippage from the right side and the leg with maximal forward slippage from the left side. For moving straight, legs that would produce the minimal difference in obstacle-induced slippage between the left and right side gets chosen at each step. For a zig-zag motion, the model chooses the activated legs to switch between counter-clockwise and clockwise turning behaviors.

This simple example demonstrates that we could extend the understanding of obstacle modulation on robot orientation beyond structured obstacle settings, to create environment-in-the-loop control strategies for more complex environments.

IV. CONCLUSIONS

In this study, we systematically examined the dynamics of a multi-legged robot's horizontal plane orientation as it traversed through a field of evenly spaced obstacles with a quasi-static trotting gait driven by an open-loop central pattern generator. Notwithstanding the absence of any body level feedback, the robot can converge to a variety of distinct, qualitatively stable steady state patterns, including equilibrium and periodic oscillations, through the repeated obstacle disturbances. These observations suggest a highly-simplified "coupled oscillator" model, which allows close prediction of robot leg-obstacle contact position pattern and the resulting steady state orientation for a variety of obstacle spacings (the external coupling frequency) and robot initial conditions (the initial phases of the oscillators). We demonstrate that the model-predicted steady-state dynamics and the underlying mechanism effectively approximate experimental measurements, and begin to allow gait-space planning for obstacle-aided navigation.

Looking ahead, the coupled oscillator model provides a mathematically tractable yet empirically effective representation that invites more careful formal reasoning about the emergence and stability of different types of synchronization patterns between locomotor phases and environment modulation. In contrast to the past traditions of the robot navigation literature, such reduced-order representations promise a computationally effective Gibsonian view of obstacles as "environmental affordances"[20], converting them into opportunities that robots can exploit to improve effectiveness in locomotion and overall mobility. We envision that extensions of the current model will open new avenues for obstacle-aided dynamic control and planning in locomotion, and eventually allow our robots to autonomously exploit different environmental affordances for different goals.

ACKNOWLEDGMENT

This research was supported by the National Science Foundation (NSF) under INSPIRE award, CISE NRI 1514882 and NRI INT award 1734355. The authors thank Matthew Kvalheim for insightful discussions on coupled oscillator representation; Sonia Roberts for helping edit the paper; and

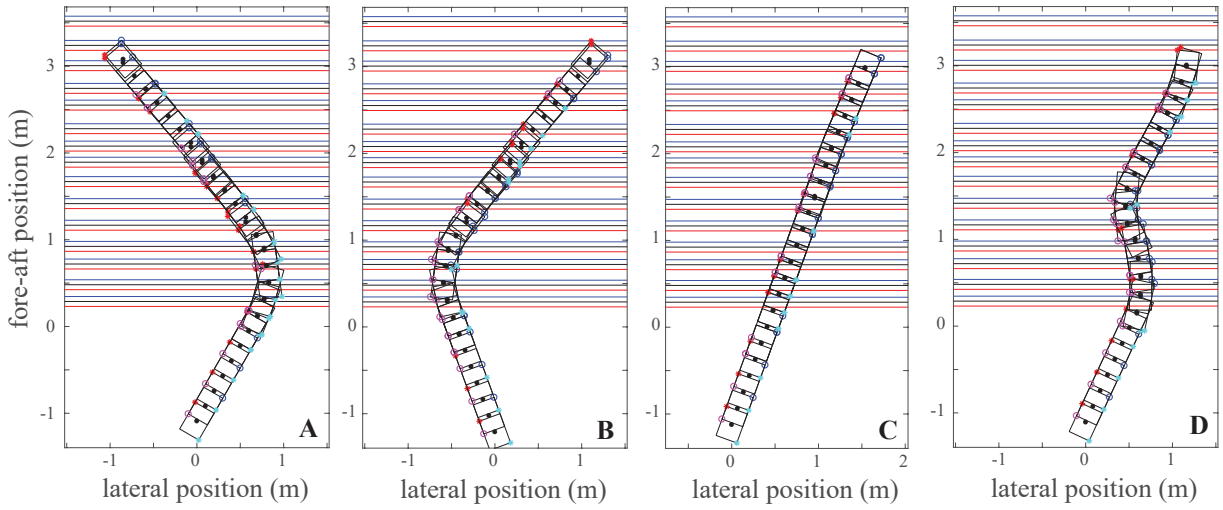

Figure 5. Gait patterns generated by the coupled oscillator model that allow a quadrupedal robot to exploit obstacle interactions to (A) turn counter-clockwise, (B) turn clockwise, (C) go straight, and (D) zig-zag, in a randomized clutter environment with obstacle spacing randomly varying between 0.06 m and 0.17 m. Marker shows which set of legs were activated at each step based on the locomotion goal. Specifically, blue circle indicates that the RF leg is activated at the step, and its position within obstacle field. Similarly, red star indicates the activation and position of the LF leg; magenta circle indicates the activation and position of the LB leg; cyan star indicates the activation and position of the RB leg. Robot body pose at each step is shown as black box.

Wei-hsi Chen for helpful discussions on figure and video improvements.

REFERENCES

[1] P. E. Schiebel, J. M. Rieser, A. M. Hubbard, L. Chen, and D. I. Goldman, "Collisional diffraction emerges from simple control of limbless locomotion," in *Conference on Biomimetic and Biohybrid Systems*. Springer, 2017, pp. 611–618.

[2] P. E. Schiebel, J. M. Rieser, A. M. Hubbard, L. Chen, D. Z. Rocklin, and D. I. Goldman, "Mechanical diffraction reveals the role of passive dynamics in a slithering snake," *Proceedings of the National Academy of Sciences*, vol. 116, no. 11, pp. 4798–4803, 2019.

[3] C. Li, A. O. Pullin, D. W. Haldane, H. K. Lam, R. S. Fearing, and R. J. Full, "Terradynamically streamlined shapes in animals and robots enhance traversability through densely cluttered terrain," *Bioinspiration & biomimetics*, vol. 10, no. 4, p. 046003, 2015.

[4] Z. Ren, R. S. Othayoth Mullankandy, and C. Li, "Legged robots change locomotor modes to traverse 3-d obstacles with varied stiffness," *Bulletin of the American Physical Society*, vol. 63, 2018.

[5] J. M. Rieser, P. E. Schiebel, A. Pazouki, F. Qian, Z. Goddard, K. Wiesenfeld, A. Zangwill, D. Negrut, and D. I. Goldman, "Dynamics of scattering in undulatory active collisions," *Physical Review E*, vol. 99, no. 2, pp. 17–19, 2019.

[6] F. Qian and D. I. Goldman, "The dynamics of legged locomotion in heterogeneous terrain: universality in scattering and sensitivity to initial conditions." in *Robotics: Science and Systems*, 2015, pp. 1–9.

[7] J. Aguilar, T. Zhang, F. Qian, M. Kingsbury, B. McInroe, N. Mazouchova, C. Li, R. Maladen, C. Gong, M. Travers, *et al.*, "A review on locomotion robophysics: the study of movement at the intersection of robotics, soft matter and dynamical systems," *Reports on Progress in Physics*, vol. 79, no. 11, p. 110001, 2016.

[8] F. Qian, T. Zhang, C. Li, P. Masarati, A. M. Hoover, P. Birkmeyer, A. Pullin, R. S. Fearing, and D. I. Goldman, "Walking and running on yielding and fluidizing ground," in *Robotics: Science and Systems*. MIT Press, 2013, p. 345.

[9] F. Qian and D. Goldman, "Anticipatory control using substrate manipulation enables trajectory control of legged locomotion on heterogeneous granular media," *Proceedings of SPIE - The International Society for Optical Engineering*, vol. 9467, 2015.

[10] B. McInroe, H. C. Astley, C. Gong, S. M. Kawano, P. E. Schiebel, J. M. Rieser, H. Choset, R. W. Blob, and D. I. Goldman, "Tail use improves performance on soft substrates in models of early vertebrate land locomotors," *Science*, vol. 353, no. 6295, pp. 154–158, 2016.

[11] S. Gart and C. Li, "Body-terrain interaction affects large bump traversal of insects and legged robots," *Bioinspiration & Biomimetics*, vol. 13, p. 026005, 2018.

[12] S. W. Gart, C. Yan, R. Othayoth, Z. Ren, and C. Li, "Dynamic traversal of large gaps by insects and legged robots reveals a template," *Bioinspiration & Biomimetics*, vol. 13, p. 026006, 2018.

[13] F. Qian and D. E. Koditschek, "An obstacle disturbance selection framework: Predicting the emergence of robot steady state orientation under repeated collisions in cluttered environments," *International Journal of Robotics Research (in revision)*, 2019.

[14] U. Saranli, M. Buehler, and D. E. Koditschek, "Rhex: A simple and highly mobile hexapod robot," *The International Journal of Robotics Research*, vol. 20, no. 7, pp. 616–631, 2001.

[15] G. D. Kenneally, A. De, and D. E. Koditschek, "Design principles for a family of direct-drive legged robots." *IEEE Robotics and Automation Letters*, vol. 1, no. 2, pp. 900–907, 2016.

[16] E. Klavins, H. Komsuoglu, R. J. Full, and D. E. Koditschek, *The Role of Reflexes versus Central Pattern Generators in Dynamical Legged Locomotion*. MIT Press, Cambridge, MA, 2002, p. 351–382.

[17] S. Revzen, D. E. Koditschek, and R. J. Full, *Towards testable neuromechanical control architectures for running*. Springer, 2009, vol. 629, p. 25–55.

[18] A. De and D. E. Koditschek, "Vertical hopper compositions for preflexive and feedback-stabilized quadrupedal bounding, pacing, pronking, and trotting," *The International Journal of Robotics Research*, vol. 37, no. 7, p. 743–778, Jun 2018.

[19] R. Altendorfer, D. Koditschek, and P. Holmes, "Stability analysis of a clock-driven rigid-body slip model for rhex," *International Journal of Robotics Research*, vol. 23, no. 10–11, p. 1001–1012, 2004.

[20] J. Gibson, "The theory of affordances the ecological approach to visual perception," pp. 127–143, 1979.